DOI: 10.1002/chem.200700260

Understanding Ribonucleotide Reductase Inactivation by Gemcitabine

Nuno M. F. S. A. Cerqueira, Pedro A. Fernandes, and Maria J. Ramos*[a]

Abstract: This paper focuses on the inhibition of ribonucleotide reductase (RNR) by gemcitabine, 2′,2′-difluoro-2′-deoxycytidine (dFdC), a deoxycytidine analogue that is a very active drug against solid tumors and is currently commercialized as gemzar. RNR inactivation is reductant-dependent and occurs in a very different way from that of other known substrate analogues. In the presence of reductants monomer R1 of RNR is inhibited, whereas in the absence of reductants the radical is lost and monomer R2 is inhibited. As inside the cell reductants are available, it is likely that R1 inactivation is the most favorable mechanism responsible for drug cytotoxicity. This inhibition pathway has been unknown to date, but we have conducted a theoretical study that has led us to the first proposal of a mechanism for RNR inhibition by dFdC in the presence of reductants.

Keywords: antitumor agents · gemcitabine · inhibitors · reaction mechanisms · ribonucleotide reductase

Introduction

Gemcitabine, 2′,2′-difluoro-2′-deoxycytidine, dFdC, is a deoxycytidine analogue that is currently showing promising results as an antiviral agent and as an anticancer drug.[1,2] It is presently employed in multiple clinical assays, alone or in combination with other drugs. The positive and encouraging results obtained in the treatment of patients with non-small-cell lung cancer[3,4] and adenocarcinoma of the pancreas, non-small-cell lung cancer, breast cancer, and ovarian cancer[5,6] have already promoted its approval by the Food and Drug Administration (FDA) and the European Agency for the Evaluation of Medicinal Products (EMEA). In Europe it has been approved additionally for the treatment of patients with bladder cancer.[7,8]

This subject is currently under intense research and over 4500 articles with gemcitabine as a keyword have already been published since it was first synthesized and evaluated in experimental tumor models by Hertel et al in 1990[9] (Figure 1). Over this time, the corresponding number of articles in the literature has displayed exponential growth. Almost 80% of these papers have cancer also as a keyword, which demonstrates the importance of this pyrimidine antimetabolite in relation to this disease.[10]

Previous studies on the metabolism of gemcitabine have demonstrated that this compound is a prodrug that is converted, by deoxycytidine kinase, to the corresponding 5′-diphosphate (dFdCDP) and triphosphate (dFdCTP).[11,12] It has been shown that these metabolites are therapeutically active agents, capable of inhibiting cellular processes and inducing cell apoptosis.[13] The cytotoxic effect of gemcitabine is attributed to a combination of two actions performed by these two metabolites.[11,14] First, dFdCDP inhibits ribonucleotide reductase (RNR), which is responsible for catalyzing the reaction that generates the deoxyribonucleotides required for DNA synthesis and repair. Therefore, inhibition of this enzyme reduces the concentration of the four DNA

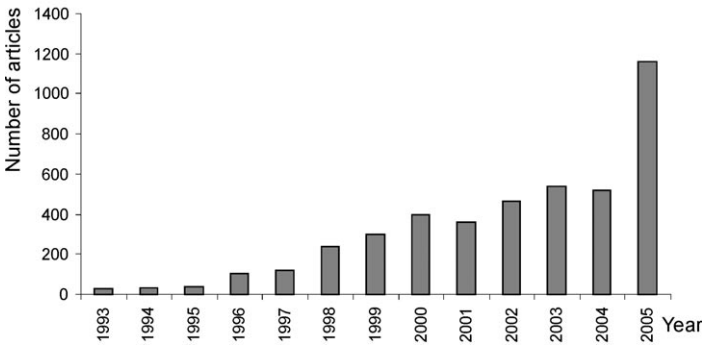

Figure 1. Number of articles with "gemcitabine" as a keyword published per year since 1990 (data acquired from the ISI Web of Knowledge).

[a] Dr. N. M. F. S. A. Cerqueira, Dr. P. A. Fernandes, Dr. M. J. Ramos
REQUIMTE, Faculdade de Ciências, Universidade do Porto
Rua Campo Alegre, 687, 4169–007 (Portugal)
Fax: (+351) 22-6082959
E-mail: mjramos@fc.up.pt

monomers in the cell moiety. Second, dFdCTP competes with the natural deoxycytidine 5-triphosphate (dCTP) for incorporation into the replicating DNA. Huang et al. showed that once one molecule of dFdCTP is incorporated, an additional deoxyribonucleotide is added to the growing DNA strands, and subsequently DNA synthesis is precluded.[15]

The decreased intracellular concentration of dCTP, caused by the inhibition of RNR, has important consequences in the cell:[16–18] 1) faster phosphorylation of dFdC to the two active forms, 2) decreased metabolic clearance of the gemcitabine nucleotides by deoxycytidine monophosphate deaminase, and 3) enhanced incorporation of dFdCTP into DNA. This self-potentiation mechanism should account for the high anticancer efficacy of dFdC relative to other nucleoside antimetabolites.

This paper focuses on the inhibition of ribonucleotide reductase promoted by gemcitabine. This enzyme has been intensively studied during the last 20 years and is currently a drug target for cancer, AIDS, and bacterial treatments, which makes this subject timely and of broad interest to many research groups.

The inhibitory mechanism of dFdC is unique in RNR,[12,19] and has several discrepancies from the other already established inhibitory mechanisms.[20,21] For example, and contrary to what happens with 2′-deoxy-2′-fluoronucleoside-5′-diphosphates (FdNDP), 2′-chloro-2′-deoxynucleoside-5′-diphosphates (CldNDP), 2′-deoxy-2′-methylenenucleoside-5′-diphosphate (CH_2FdNDP), and 2′-deoxy-2′-mercaptonucleoside-5′-diphosphate (SHdNDP), the presence or absence of reductants does not preclude enzyme inhibition. The formation of the common furanone derivative with a characteristic UV/visible absorbance band at 320–330 nm is not observed. Further electron paramagnetic resonance (EPR) studies show that, in the absence of reductants, an unusual stable radical species is observed with no equivalent amongst other similar RNR inhibitors.

Previous theoretical work[22] was devoted to the study of the gemcitabine inhibitory mechanism in the absence of reductants. However, as inside the cell reductants are available, it is likely that R1 inactivation is the most favorable mechanism responsible for drug cytotoxicity in vivo. Taking this into account, this paper is devoted to the unknown inhibition mechanism that occurs in dFdC, in the presence of reductants. Some experimental results are available on this subject, however, this inhibitory pathway is still unclear.

Theoretical Approach

Theoretical model: Small models were used to simulate the desired reactions. Cysteine and glutamate residues were modeled as methylthiols and formate molecules, respectively. The dFdCDP molecule was modeled without the C-5′ atom, the phosphates, and the cytosine groups. The adequacy of these models was demonstrated in earlier works.[20,23,24] Furthermore, it was shown recently that the difference in either activation energy or reaction energy between a model that includes explicitly the whole R1 monomer at the QM/MM level (12000 atoms) and a smaller model the size of the present one (up to 40 atoms), embedded in a dielectric medium with $\varepsilon = 4$, is less than 1.5 kcal mol^{-1}. Nevertheless, special care was taken here so that the relative position of each residue could be reproduced in the X-ray structure,[25] and the most important direct interactions were included explicitly in the model. The other, long-range interactions coming from the bulk of the protein were calculated by dielectric continuum methods.[26] These kinds of models allow for the evaluation of the energy with a higher level of theory, in contrast to the practical use of QM/MM methodologies.

Theoretical methods: Density functional theory (DFT) was used in all geometry optimizations. The chosen functional was the B3LYP with the 6–31G(d) basis set, as included in the Gaussian 03 package.[27] Final energies were corrected by single-point energy calculations at a very high level of theory, namely the QCISD(T)[28] level, and with a larger polarized valence triple-ξ aug-cc-pVTZ basis set.[29,30]

Frequency calculations confirmed the nature of each stationary point, that is, an energy minimum with all frequencies real or, in the case of a transition state, with only one imaginary frequency. The transition states were verified to connect the reactants and products of interest through internal reaction-coordinate calculations (IRC). Zero-point, thermal, and entropic effects ($T = 298.15$ K, $P = 1$ bar) were added to the calculated energies.

A scale factor of 0.9804 was used to eliminate known systematic errors in zero-point energies and thermal-energy corrections. A problem associated with the unrestricted wave functions is spin contamination. The expected values of the spin in the optimized structures never exceeded 0.76 and after annihilation they returned to the desired value of 0.750.

The atomic spin-density distributions were calculated at the B3LYP level by employing a Mulliken population analysis, using the basis set 6–311++G (3df,3pd).

A polarized-continuum model was employed, referred as C-PCM, as implemented in Gaussian 03,[27] to calculate the final energies. In this approach, the continuum is modeled as a conductor, instead of a dielectric. This simplifies the electrostatic computations, and corrections are made a posteriori for dielectric behavior. A dielectric constant of four has shown previously to provide theoretical results hat are in agreement with their experimental counterparts, taking care of the protein ($\varepsilon = 3$) and the buried waters environments ($\varepsilon = 80$).[23]

Results and Discussion

RNR is a ubiquitous enzyme, expressed in a wide variety of organisms. *E. Coli* ribonucleotide diphosphate reductase, from Class Ia is one of the most characterized and investi-

gated enzymes and it serves as a prototype for the mammalian protein.

RNR Class Ia is composed of a complex of two subunits from which the enzymatic activity is dependent (Figure 2). One of the subunits, R1, controls the overall enzyme activity and is composed of two identical monomers, each one lodging one active site containing five conserved residues (Cys225, Asn437, Glu441, Cys439, and Cys462), and three independent allosteric sites. The other subunit, R2, is also composed of two identical monomers, each one containing a stable neutral tyrosyl free radical coupled to a binuclear iron cluster that is required for its generation.

RNR can be inhibited at an early stage during the transcription of mRNA (antisense inhibitors) or when the protein is already formed, either by precluding subunit dimerization (dimerization inhibitors) or by direct attack on protein R1 or R2. Gemcitabine is part of the latter group and is capable of inhibiting protein R1 and protein R2. From the large database of RNR inhibitors, gemcitabine is the most potent mechanism-based inhibitor known to date.[31] The puzzling inhibitory mechanism of gemcitabine has been under discussion for decades and, although several pieces of this puzzle have been unraveled, the solution remains far from clear.[32–34]

Recently, Pereira et al.[22] showed that the gemcitabine inhibitory mechanism, in the absence of reductants, is similar to that of the natural reduction pathway (Scheme 1). The first part of the mechanism involves the abstraction of the H-3′ atom by Cys439 (**1**) and the hydrogen-atom transfer from OH-3′ to Glu441 (**2**). This sequence of steps occurs, in most of the substrate analogues, as two consecutive steps but, in the case of gemcitabine, the hydrogen-atom transfer, promoted by Glu441, occurs prior to the Cys439 abstraction. This can be explained by the electrowithdrawing nature of the groups attached to the C-2′ atom that influence the acidity of the neighboring C-3′ atom. The third step involves the release of the fluorine atom that is attached to the bottom face of the substrate (**3**). This step is assisted by the protonated Cys225 and yields one molecule of HF. In the fourth step, there is a hydrogen-atom transfer between Cys225 and Cys462 (**4**) and in the next step this hydrogen becomes attached to carbon C-2′ of the substrate. At this stage, both sulfur atoms become connected by an anionic-radical disulfide bridge, which is experimentally detected by EPR spectroscopy (**5**). As in the natural substrate, the next step involves the oxidation of both cysteines with the simultaneous proton transfer from Glu441 to the O-3′ atom of the substrate (**6**). In the final step, the dissociation of the other fluorine atom with the help of Cys439 occurs, generating another molecule of HF (**7**). We propose that the mechanism must diverge subsequently at this point, depending on the availability of reductants, according to Scheme 2.

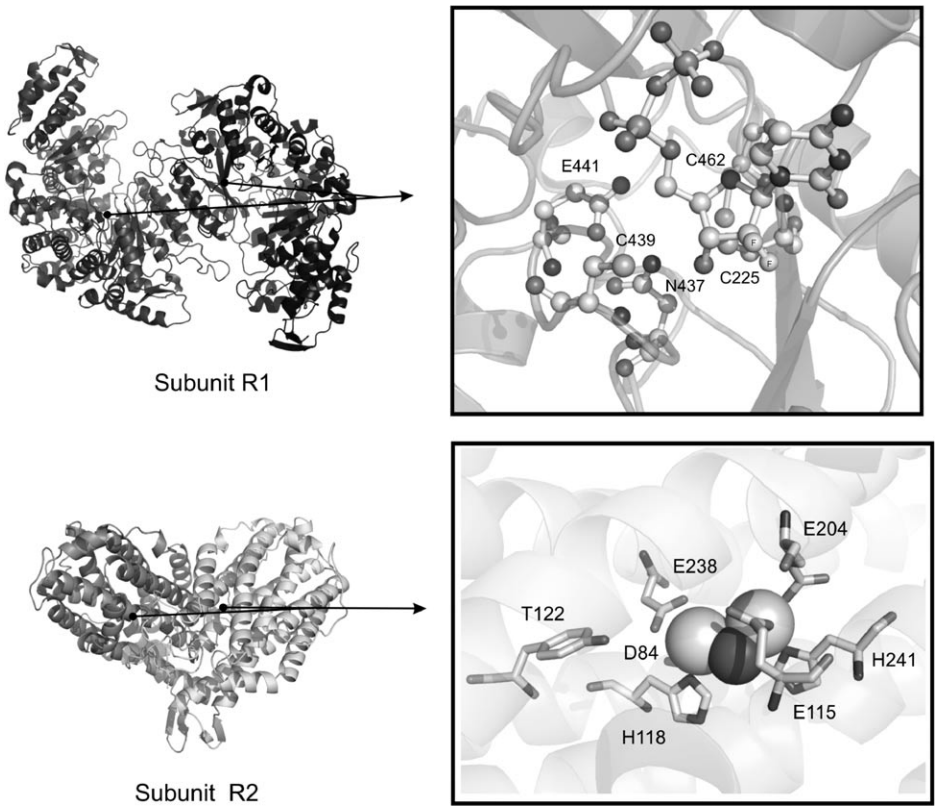

Figure 2. Representation of subunits R1 and R2. Top: Key residues of the ribonucleotide reductase (RNR) active site that is located at subunit R1 (location marked with black spots in Figure 2). Bottom: Organometallic complex located in subunit R2 at which the radical is generated (location marked with black spots in Figure 2).

It is experimentally known that in the absence of reductants the inhibition is due predominantly to the reduction of the radical and, therefore, the inhibition of monomer R2. Monomer R1 remains active, but the overall activity of the enzyme is precluded. This inactivation is characterized by the detection of an unusual EPR signal that is believed to be substrate based.[33,34] The spectrum is characterized by two hyperfine interactions of the same magnitude with nuclei of spin 1/2. The location of the radical is uncertain, but theoretical results have shown that the radical should be located at the C-4′ atom, with two hydrogen atoms, connected to C-5′, being the ones responsible for the hyperfine interaction. The formation of this radical could be possible in a couple of steps

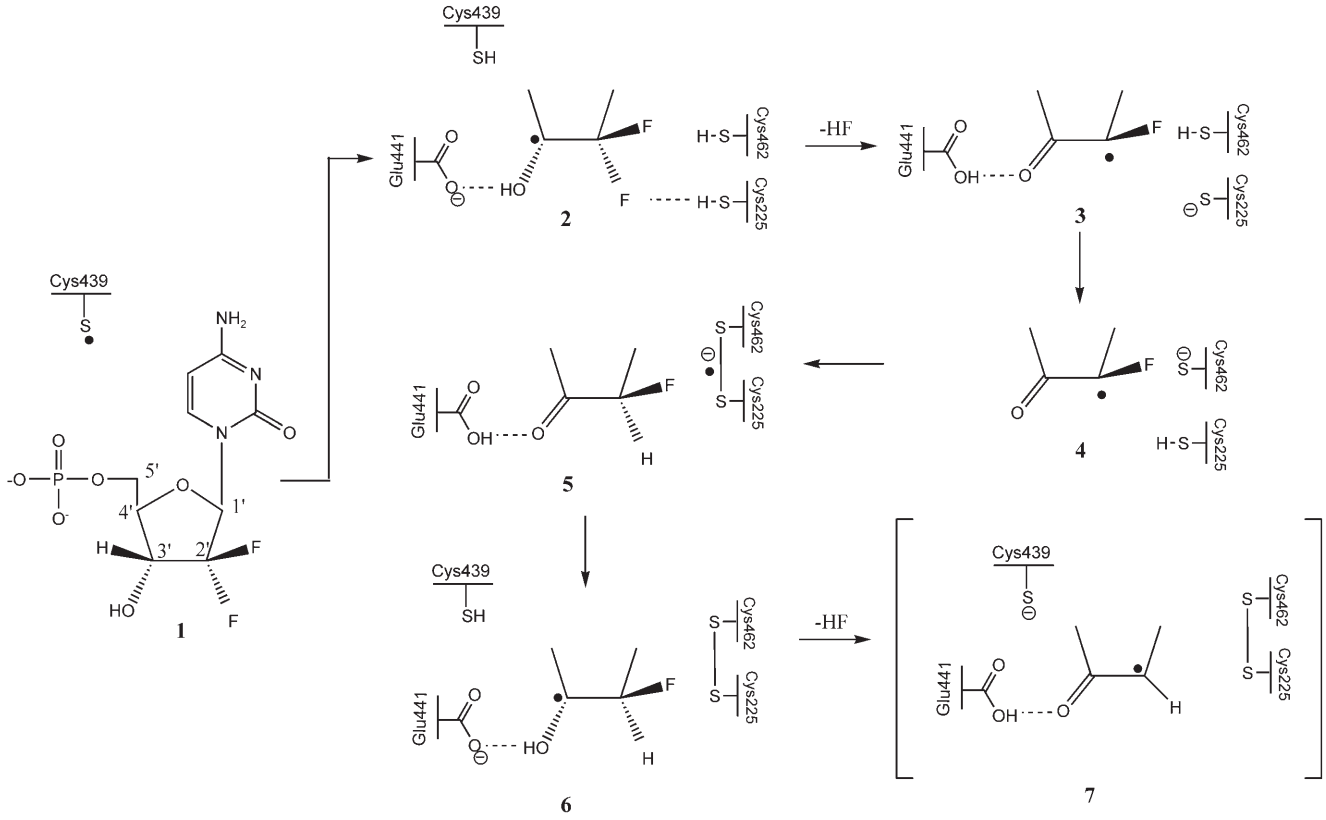

Scheme 1. RNR inhibitory mechanism promoted by gemcitabine, up to the formation of the Cys225–Cys462 disulfide bridge.

starting from structure **7** (pathway C, Scheme 2). From this point, it was proposed by Pereira et al. that the first step would involve the hydrogen-atom transfer from Cys439 to C-2′ of the substrate. Subsequently, there is a hydrogen-atom abstraction from C-4′ in the substrate by Cys439. This reaction is possible due to the reactivity of the C-4′atoms and the very stable nucleotide-based radical that is formed in the product of the reaction, and definitely prevents the regeneration of the tyrosyl radical in protein R2.

Experimental results have shown that in the presence of reductants protein R1 is inhibited, whereas protein R2 remains active, contrary to what happens in the absence of reductants. As inside the cell reductants are available, it is likely that R1 inactivation is the most favorable mechanism responsible for drug cytotoxicity, which increases the interest in this inhibition process.

Experimentally, the inactivation is proposed to be distinctive from the majority of other 2′-substituted nucleotides, involving reactive species that are generated within the active site (protein R1) and never leave this site although reductants are available. This theory is supported because the formation of a chromophore in solution, common amongst other substrate-analogue inhibitors, is not observed in gemcitabine. Furthermore, the unique detection of cytosine and fluorine molecules in solution, but not of pyrophosphate or sugar derivatives, suggests the alkylation of species inside the active site.

To unravel the inhibitory mechanism in the presence of reductants we studied several possible pathways, as well as their energetics, and tried to find the most favorable pathway from a kinetic point of view. Here we discuss the three most favorable pathways that we followed.

As mentioned above, the point after which the mechanism is proposed to diverge depending on the availability of reductants, is structure **7**. At this point the radical is located at the C-2′ atom of the substrate and the charge at Cys439. The Glu441 is protonated, both cysteines are connected by a disulfide bridge, and the substrate is found as a radical keto-deoxyribonucleotide.

In the presence of reductants, the reduction of cysteines Cys225 and Cys462 becomes a possibility. The commonly accepted dithiol/disulfide exchange mechanism involves a nucleophilic attack of a thiolate on the disulfide complex,[35] generating a cross-linked intermediate, as depicted in Scheme 3. Accordingly, Cys225 becomes necessarily anionic. Furthermore, at this stage and taking in account the pK_a of thiols and of HF, Cys439 remains protonated.

From this point on, three possible pathways can be envisioned to trap the nucleotide inside the active site and generate a covalent adduct (Scheme 2, pathway C): the anionic Cys225 adds to 1) atom C-2′ (pathway A) or 2) atom C-3′ of the substrate (pathway B), or there is a hydrogen-atom transfer from Cys439 to atom C-3′ of the substrate. The latter pathway (pathway C) is the same as the one proposed to occur in the absence of reductants.

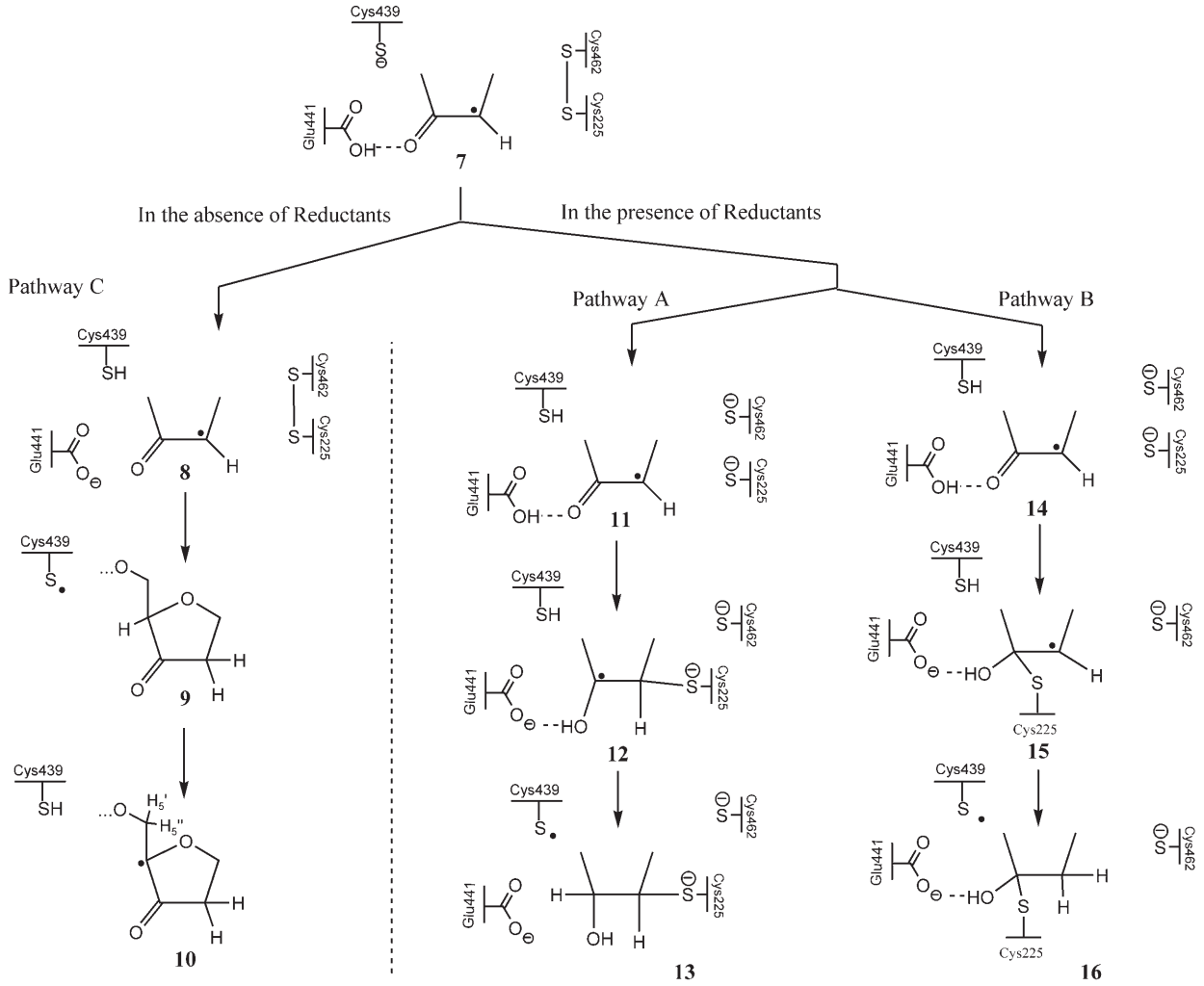

Scheme 2. Proposed pathways A,B,C starting at a point after which the inhibitory mechanism promoted by gemcitabine diverges, depending on the availability of reductants.

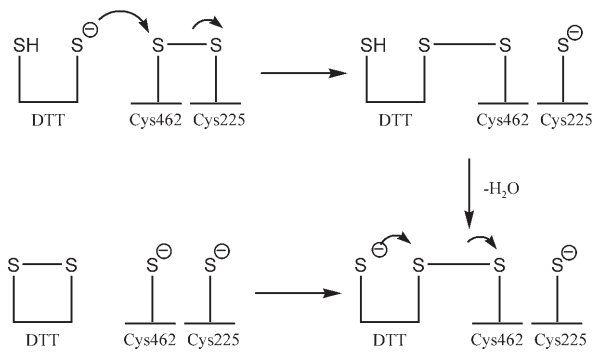

Scheme 3. Mechanism of reduction of Cys225.

To study these pathways we built models capable of simulating the modeled reactions with a very high level of theory. Because a compromise between the size of the model and the accuracy of the results is necessary, we used systems which do not contain more than 40 atoms. This choice was made because, in RNR, the size of the model is not important for this kind of study. This conclusion is based on our past experience in which several steps of the normal reduction pathway of the RNR mechanism were studied by using increasing sizes of the modeled enzyme.[20,23,24] The results showed that there is little significant difference between the calculated energies obtained for the full enzyme and for this kind of model; only a difference of 1.5 kcal mol^{-1} was observed.[23] The advantage of this procedure is to allow for the evaluation of the energy with a higher level of theory and, therefore, with much more accuracy, as an alternative to the use of QM/MM methodologies.

Theoretical calculations showed that the starting points of pathways A and B are very similar. The anionic Cys225 is very close to the substrate and two positions are available for a nucleophilic attack: the C-2′ carbon atom at a distance of 2.75 Å and the C-3′ carbon atom at a distance of 3.25 Å. The hydroxyl group of Glu441 is in close contact with the ketone group of the substrate, with the hydrogen atom only 1.51 Å away. The spin density and the charge are shared between the substrate (0.42 and −0.58 a.u., respectively) and

Cys225 (0.59 and −0.50 a.u., respectively). This shared charge/spin distribution together with the observed bond lengths between the atoms C-2′–C-3′ and C-3′–O-3′ indicates the existence of two resonance structures (Scheme 4).

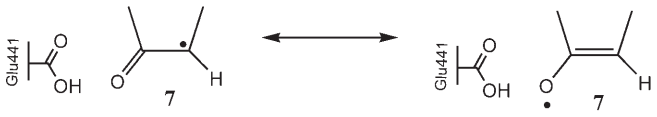

Scheme 4. Resonance structures of molecule **7**.

However, at the obtained minimum, the distance between atoms C-3′ and O-3′ (1.28 Å), which is typical of partial double-bond lengths comprising a carbon and an oxygen (1.29 Å), the distance between atoms C-2′ and C-3′ (1.38 Å), shorter than a common single-bond length (1.64 Å) and closer to a double-bond length between two carbons (1.34 Å), and the charge and spin-density concentration in the substrate at atoms C-3′and O-3′, show that molecule **7a** is the most stable structure in that particular environment.

Step 1: In pathway A, the transition state for the nucleophilic addition of the Cys225 thiolate is characterized by a unique imaginary frequency of $-968.59\,cm^{-1}$ that involves (Figure 3): 1) the addition of Cys225 to carbon atom C-2′ of the substrate, 2) the proton transfer from Glu441 to the ketone group of the substrate, and 3) the radical transfer to carbon atom C-2′ of the substrate. The spin density is shared between the substrate (0.61 a.u.) and Cys225 (0.39 a.u.), and the charge is located mainly at Glu441 (−1.02 a.u.). Interestingly, in the transition state the substrate shows a lack of electronic density (0.54 a.u.) contrary to what happens with Cys225 (−0.46 a.u). At this stage, Cys225 is almost bonded to the carbon atom C-2′ of the substrate (2.19 Å) and the hydroxyl group is already formed at atom C-3′ of the substrate, with the hydrogen atom kept at 1.34 Å from Glu441. The activation free energy involved in this process is very small, corresponding to $2.48\,kcal\,mol^{-1}$.

In pathway B, Cys225 adds to carbon atom C-3′ of the substrate. The transition state involves two simultaneous transformations around carbon C-3′(Figure 3): 1) the addition of the anionic Cys225 to atom C-3′ and, similarly to the other pathway, 2) the hydrogen-atom transfer from Glu441 to the ketone group of the substrate. The radical remains located at carbon C-3′ (0.69 a.u.) of the substrate and, as in pathway A, the charge becomes located at Glu441 (−1.04 a.u.) because the proton is already transferred to atom O-3′. The anionic Cys225 is aligned with atom C-3′ at 2.17 Å. The activation free energy in this step is small ($6.16\,kcal\,mol^{-1}$), but higher by about $4\,kcal\,mol^{-1}$ than the corresponding one in the other pathway. Despite being small, this energy reflects the lower stability of intermediate **12** relative to structure **9**. This is due mainly to the presence of the hydroxy group at carbon C-3′ that makes this step less favorable, from a stereochemical point of view.

Due to the different positions of the nucleophilic attack in the two pathways, two different structures are obtained as products. In pathway A, Cys225 is bonded to carbon C-2′ of

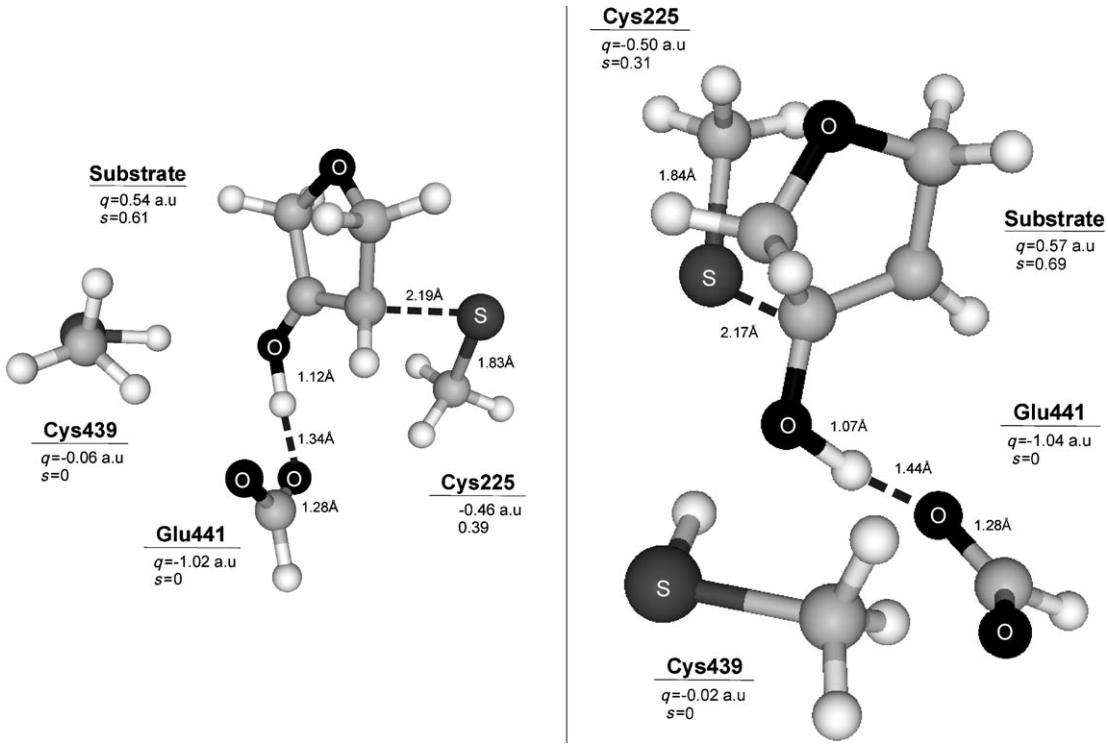

Figure 3. Transition state in the first step of pathway A (left) and pathway B (right).

the substrate (C-2′–S = 1.85 Å). The spin is mainly located at carbon C-3′ of the substrate (0.79 a.u,) and the charge remains located at Glu441 (−1.03 a.u.). The reaction is exothermic, and the products are more stable than the reactants (−2.36 kcal mol^{-1}). In pathway B, Cys225 bonds to atom C-3′ of the substrate (C-3′–S = 1.97 Å). The spin remains located at the C-2′ carbon atom of the substrate (1.06 a.u.) and the charge is concentrated at Glu441 (−1.03 a.u.). Contrary to what happens in pathway A, the reaction is endothermic, +1.41 kcal mol^{-1}.

The zero-point energy, thermal corrections, and continuum effect (already included in the above-mentioned energy values) increase the value by +1.34 kcal mol^{-1} for the activation energy and by +2.46 kcal mol^{-1} for the reaction free energy in pathway A, and by +0.97 kcal mol^{-1} and +0.70 kcal mol^{-1}, respectively, in pathway B.

Step 2: Following pathway A, the next step involves the hydrogen-atom transfer from Cys439 to carbon C-3′ of the substrate, generating the deoxyribonucleotide derivative, but with Cys225 bonded to atom C-2′. This step is similar to the last step of the normal reduction pathway and from which the regeneration of the radical, experimentally observed, is achieved. In the reactants, the thiol group of Cys439 is found 2.70 Å away from carbon C-3′ of the substrate. The spin is located at carbon C-3′ (0.79 a.u.) and the charge at Glu441 (1.04 a.u.). At the transition state, the hydrogen-atom transfer occurs in an almost perfectly collinear fashion with an S-H-C angle of 175°, with the hydrogen atom located 1.53 Å away from the sulfur atom (Cys439) and at 1.45 Å from carbon C-3′ (Figure 4). The spin distribution is divided between the sulfur atom (0.21 a.u.) and carbon C-3′ (0.69 a.u.), revealing the proximity and interaction of both atoms. In the optimized geometry of the products, the spin density is located at Cys439 (0.97 a.u.) and the charge remains located at Glu441 (−1.08a.u.). The hydrogen is now bonded to carbon C-3′ of the substrate (1.10 Å) and at 4.11 Å from the sulfur atom of Cys439. The calculated free-energy barrier necessary to achieve the transition state is +13.17 kcal mol^{-1} and the reaction free energy is −11.67 kcal mol^{-1}. The zero-point, thermal corrections, and continuum effect increased the barrier by +1.77 kcal mol^{-1} for the activation energy and by +2.89 kcal mol^{-1} for the reaction free energy.

In pathway B, the final step involves the hydrogen-atom transfer from Cys439 to atom C-2′ of the substrate. This step is very similar to the last step of the inhibition reaction pathways of both CldNDP and FdNDP in which it was shown that Cys439 has sufficient mobility to reach carbon C-2′ of the substrate.[36] In the reactants, the spin density is located at carbon C-2′ (0.85 a.u.) of the substrate, being the thiol group of Cys439 at 3.39 Å from this center. The charge remains located at Glu441 (−1.04 a.u.). At the transition state, the distance between carbon C-2′ and the hydrogen atom is 1.56 Å, and the thiol bond length is elongated to 1.49 Å (1.36 Å in the reactants) (Figure 4).The spin density is shared between carbon C-3′ of the ribonucleotide (0.62 a.u.) and the sulfur of Cys439 (0.23 a.u.), showing the proximity and interaction of both atoms. In the products, we observe the presence of the thiyl group (spin density of 0.97 a.u.) in Cys439 and the new C–H bond (1.09 Å) at the substrate. The activation energy required for this step is +16.0 kcal mol^{-1} and the free energy of reaction is −10.90 kcal mol^{-1}. The zero-point energy, thermal corrections, and continuum

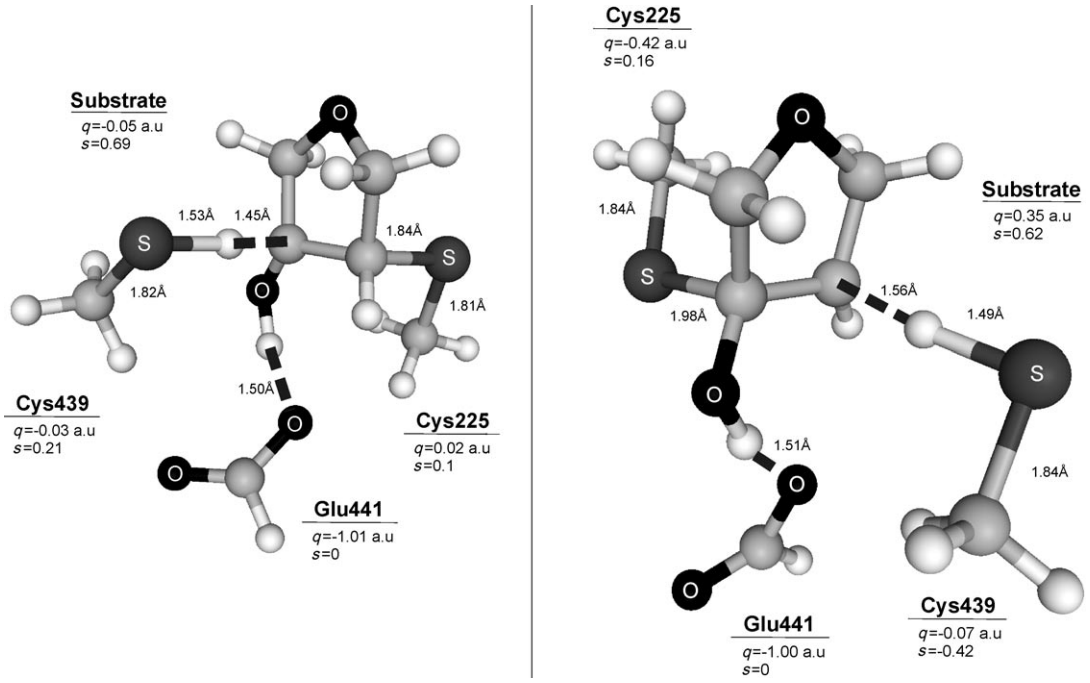

Figure 4. Transition state in the second step of pathway A (left) and pathway B (right).

effect increase the value by $+1.08\,kcal\,mol^{-1}$ for the activation energy and $+5.65\,kcal\,mol^{-1}$ for the reaction free energy (Figure 5).

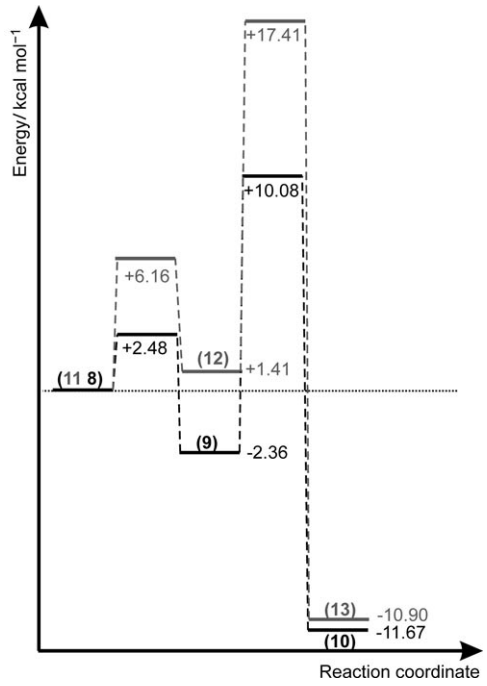

Figure 5. Free energies, ΔG, of the discussed pathways, subsequent to the point at which the inhibitory mechanism diverges, depending on the availability of reductants (pathway A, black; pathway B, gray). Structures shown in Scheme 2 are also identified.

During the first step of the inhibitory mechanism, when reductants are present, it is not clear which pathway, A or B, is favored, as both the activation energy ($4\,kcal\,mol^{-1}$) and the reaction energies ($\approx 3\,kcal\,mol^{-1}$) are rather small. In the second step, irrespective of the pathway followed, the final products have similar stabilities ($-10.90\,kcal\,mol^{-1}$ for structures **13** and $-11.67\,kcal\,mol^{-1}$ for structure **10**). However, the activation energy in pathway A is smaller by about $3\,kcal\,mol^{-1}$, which makes this pathway more favorable kinetically. Furthermore, the inhibitory mechanism of pathway A has several advantages over pathway B, from both a stereospacial and a stereochemical point of view. For example, the bond length between the sulfur atom from Cys225 and the carbon atom from the substrate (C-2′ in pathway A and C-3′ in pathway B) is smaller in pathway A (1.85 Å) than in pathway B (1.97 Å), which may make the former compound less stable than the latter. These facts might cause pathway A to be preferred when reductants are available.

The studied pathways allow us to elucidate why, in the presence of reductants, stoichiometric inactivation of R1 is distinct from the majority of the other 2′-substituted 2′-deoxynucleotides, and the formation of new species in solution, such as the furanone derivative (besides cytosine and both fluorines), is not observed. Cys225 plays the main role in this process and its covalent addition to carbon atoms C-2′ or C-3′ of the substrate was shown to be possible, which precludes the dissociation of the gemcitabine derivative from the active site into the solution. The involvement of Cys225 in the alkylation of ribonucleotides is not new and a similar behavior was also proposed in the inhibitory mechanism of CH_2FdNDP[33].

Conclusions

This study has allowed us to unravel the inhibitory mechanism of gemcitabine in the presence of reductants and to clarify differences and similarities when reductants are absent. We can conclude that both inhibitory mechanisms have similar pathways at an initial stage but diverge after the formation of the radical-ketodeoxyribonucleotide **7**. This explains why the mode of RNR inactivation by gemcitabine is reductant dependent.

In the presence of reductants we propose that Cys225 is responsible for substrate alkylation within the active center. This explains why for each equivalent of gemcitabine no other molecule is detected in solution besides cytosine and two molecules of fluorine. We have studied several inhibitory pathways and have observed that in the presence of reductants two competitive inhibitory pathways are available. From a stereospacial and a stereochemical point of view, we can conclude that the nucleophilic attack of the anionic Cys225 on carbon C-2′ is the most favorable pathway.

With this study we are able to explain why gemcitabine is the most efficient inhibitor relative to the other RNR substrate-analogue inhibitors. The main reason deals with the fact that once gemcitabine binds into the active site it no longer dissociates into the solution, because it becomes trapped by covalent bonding to Cys225. With the other inhibitors, the most common inhibitory mechanism involves the formation of a ketodeoxyribonucleotide derivative. However, in these cases, this compound must dissociate into the solution, where it decomposes to a methylene-3(2H)-furanone derivative that inhibits the enzyme only when reductants are absent, a situation that does not occur in vivo.

Acknowledgement

Fundação para a Ciência e Tecnologia (Ph.D. Project POCTI/35736/99, Portugal) is gratefully acknowledged for financial support.

[1] T. Szekeres, M. Fritzer-Szekeres, H. L. Elford, *Crit. Rev. Clin. Lab. Sci.* **1997**, *34*, 503–528.
[2] V. Bianchi, S. Borella, F. Calderazzo, P. Ferraro, L. Chieco Bianchi, P. Reichard, *Proc. Natl. Acad. Sci. USA* **1994**, *91*, 8403–8407.
[3] M. Fukuoka, M. Takada, A. Yokoyama, Y. Kurita, H. Niitani, *Semin. Oncol.* **1997**, *24*, S7-42–S47-46.
[4] F. A. Shepherd, R. P. Abratt, H. Anderson, U. Gatzemeier, G. Anglin, J. Iglesias, *Semin. Oncol.* **1997**, *24*, S7-50–S57-55.
[5] J. M. Plate, A. E. Plate, S. Shott, S. Bograd, J. E. Harris, *Cancer Immunol. Immunother.* **2005**, *54*, 915–925.

[6] P. Prost, M. Ychou, D. Azria, *Bull Cancer* **2002**, *89, Spec No.* S91–95.
[7] H. von der Maase, *Semin. Oncol.* **2001**, *28*, 1–3.
[8] S. Nawrocki, T. Skacel, I. Skoneczna, *Expert Opin. Pharmacother.* **2002**, *3*, 671–679.
[9] L. W. Hertel, G. B. Boder, J. S. Kroin, S. M. Rinzel, G. A. Poore, G. C. Todd, G. B. Grindey, *Cancer Res.* **1990**, *50*, 4417–4422.
[10] N. M. Cerqueira, P. A. Fernandes, M. J. Ramos, *Recent Pat. Anti-Cancer Drug Discovery* **2007**, *2*, 11–29.
[11] C. L. van der Wilt, J. R. Kroep, A. M. Bergman, W. J. Loves, E. Alvarez, I. Talianidis, S. Eriksson, C. J. van Groeningen, H. M. Pinedo, G. J. Peters, *Adv. Exp. Med. Biol.* **2000**, *486*, 287–290.
[12] R. L. Merriman, L. W. Hertel, R. M. Schultz, P. J. Houghton, J. A. Houghton, P. G. Rutherford, L. R. Tanzer, G. B. Boder, G. B. Grindey, *Invest. New Drugs* **1996**, *14*, 243–247.
[13] C. M. Galmarini, J. R. Mackey, C. Dumontet, *Leukemia* **2001**, *15*, 875–890.
[14] A. M. Bergman, P. P. Eijk, V. W. Ruiz van Haperen, K. Smid, G. Veerman, I. Hubeek, P. van den Ijssel, B. Ylstra, G. J. Peters, *Cancer Res.* **2005**, *65*, 9510–9516.
[15] I. Climent, B. M. Sjoberg, C. Y. Huang, *Biochemistry* **1991**, *30*, 5164–5171.
[16] V. Gandhi, S. Mineishi, P. Huang, A. J. Chapman, Y. Yang, F. Chen, B. Nowak, S. Chubb, L. W. Hertel, W. Plunkett, *Cancer Res.* **1995**, *55*, 1517–1524.
[17] V. Gandhi, S. Mineishi, P. Huang, Y. Yang, S. Chubb, A. J. Chapman, B. J. Nowak, L. W. Hertel, W. Plunkett, *Semin. Oncol.* **1995**, *22*, 61–67.
[18] S. Miura, Y. Yoshimura, H. Satoh, S. Izuta, *Jpn. J. Cancer Res.* **2001**, *92*, 562–567.
[19] V. Heinemann, Y. Z. Xu, S. Chubb, A. Sen, L. W. Hertel, G. B. Grindey, W. Plunkett, *Mol. Pharmacol.* **1990**, *38*, 567–572.
[20] N. M. F. S. A. Cerqueira, P. A. Fernandes, L. A. Eriksson, M. J. Ramos, *J. Mol. Struct. THEOCHEM* **2004**, *709*, 53–65.
[21] N. M. Cerqueira, S. Pereira, P. A. Fernandes, M. J. Ramos, *Curr. Med. Chem.* **2005**, *12*, 1283–1294.
[22] S. Pereira, P. A. Fernandes, M. J. Ramos, *J. Comput. Chem.* **2004**, *25*, 1286–1294.
[23] N. M. Cerqueira, P. A. Fernandes, L. A. Eriksson, M. J. Ramos, *Biophys. J.* **2006**, *90*, 2109–2119.
[24] N. M. Cerqueira, P. A. Fernandes, L. A. Eriksson, M. J. Ramos, *J. Comput. Chem.* **2004**, *25*, 2031–2037.
[25] H. Xu, C. Faber, T. Uchiki, J. Racca, C. Dealwis, *Proc. Natl. Acad. Sci. USA* **2006**, *103*, 4028–4033.
[26] P. A. Fernandes, M. J. Ramos, *Chem. Eur. J.* **2003**, *9*, 5916–5925.
[27] M. J. Frisch, G. W. Trucks, H. B. Schlegel, G. E. Scuseria, M. A. Robb, J. R. Cheeseman, V. G. Zakrzewski, J. A. Montgomery, Jr., R. E. Stratmann, J. C. Burant, S. Dapprich, J. M. Millam, A. D. Daniels, K. N. Kudin, M. C. Strain, O. Farkas, J. Tomasi, V. Barone, M. Cossi, R. Cammi, B. Mennucci, C. Pomelli, C. Adamo, S. Clifford, J. Ochterski, G. A. Petersson, P. Y. Ayala, Q. Cui, K. Morokuma, D. K. Malick, D. A. Rabuck, K. Raghavachari, J. B. Foresman, J. Cioslowski, J. V. Ortiz, A. G. Baboul, B. B. Stefanov, G. Liu, A. Liashenko, P. Piskorz, I. Komaromi, R. Gomperts, R. L. Martin, D. J. Fox, T. Keith, M. A. Al-Laham, C. Y. Peng, A. Nanayakkara, C. Gonzalez, M. Challacombe, P. M. W. Gill, B. Johnson, W. Chen, M. W. Wong, J. L. Andres, C. Gonzalez, M. Head-Gordon, E. S. Replogle, and J. A. Pople in *Gaussian 03*, Gaussian, Inc., Pittsburgh, **2003**.
[28] J. A. Pople, M. Head-Gordon, K. Raghavachari, *J. Chem. Phys.* **1987**, *87*, 5968–5975.
[29] R. A. Kendall, T. H. Dunning, R. J. Harrison, *J. Chem. Phys.* **1992**, *96*, 6796–6806.
[30] D. E. Woon, T. H. Dunning, *J. Chem. Phys.* **1993**, *98*, 1358–1371.
[31] C. H. Baker, J. Banzon, J. M. Bollinger, J. Stubbe, V. Samano, M. J. Robins, B. Lippert, E. Jarvi, R. Resvick, *J. Med. Chem.* **1991**, *34*, 1879–1884.
[32] F. H. Hausheer, N. D. Jones, P. Seetharamulu, U. C. Singh, J. B. Deeter, L. W. Hertel, J. S. Kroin, *Comput. Chem. Eng.* **1996**, *20*, 459–467.
[33] W. A. van der Donk, G. Yu, L. Perez, R. J. Sanchez, J. Stubbe, V. Samano, M. J. Robins, *Biochemistry* **1998**, *37*, 6419–6426.
[34] D. J. Silva, J. Stubbe, V. Samano, M. J. Robins, *Biochemistry* **1998**, *37*, 5528–5535.
[35] P. A. Fernandes, M. J. Ramos, *J. Am. Chem. Soc.* **2003**, *125*, 6311–6322.
[36] N. M. Cerqueira, P. A. Fernandes, M. J. Ramos, *J. Phys. Chem. B* **2006**, *110*, 21272–21281.

Received: February 13, 2007
Revised: May 7, 2007
Published online: July 18, 2007

